

## Chapter 3

# Effects of localised shearing on crystal growth and nucleation

As outlined in Chapter 1, the original outline of the PhD was to investigate the possibility of using optical tweezing as a means of initiating and controlling nucleation by generating fluid flow within a small droplet of supersaturated solution. The goal of which would be to understand the influence of shearing on nucleation at a micro level as compared to larger scale results. It has been shown that for macro-scale systems, the likelihood of nucleation increases to a maximum value under increased shearing [1, 2]. Theoretical research into the matter identified two competing effects that effect a crystal in moving fluid fields; firstly, nucleation is enhanced due to the increased mass transfer of solute material; and secondly, shear flow against the crystal surface leading to a decrease in growth [2]. These two competing effects are validated by experimental work using glycine solutions, showing that beyond a certain shear rate the nucleation

rate is reduced [1]. In this chapter I outline the optical tweezer equipment used during this PhD, the initial attempts made to induce nucleation via optical rotation, and the impact of a moving beam on the crystal growth of a newly formed nucleus.

### 3.1 Optical Tweezer Equipment

In general, all optical tweezers require a laser driver, two microscope objectives (one for trapping and one for imaging), and a means of controlling the position of the loaded sample. While there are other pieces of equipment used in modern tweezer experiments these are the bare minimum requirements for any optical tweezer. The laser used for this project was a 1064 nm near infrared laser - provided by CNI Lasers – that has an adjustable power supply to vary the energy output of the laser - the remaining optics were supplied by Thor Labs. Experimental work has shown that the trapping efficiency increases with beam diameter up until it exceeds  $\frac{2}{3}D_{obj}$  [3] where  $D_{obj}$  is the diameter of the objective aperture. To expand the beam front we utilise a Galilean beam expansion arrangement (indicated by  $f_1$ , and  $f_2$ ) as recommended for high power laser applications. In our initial experiments the beam expansion provides a  $4\times$  magnification; however, in later experiments where we utilise a galvano-mirror the beam expansion is  $3\times$  and then the 4f correlator provides a further  $1.25\times$  magnification (using  $f_3$  and  $f_4$ ) - where the magnification is given by.

$$\frac{D_2}{D_1} = \frac{f_2}{f_1} \quad (3.1)$$

It should be noted that the galvano-mirror requires the use of a Keplerian beam ex-

pansion arrangement which reduces the transmitted laser power due to localised heating of the air. Afterwards the laser is passed through a dichroic mirror that separates incoming infrared and visible light, this is to prevent the laser from damaging the CCD camera used for imaging the trapping plane. The laser is then focused to a diffraction limited spot by a 1.25 NA objective. By increasing the numerical aperture of the objective, the gradient force at the focal point is increased; the trade-off being that the for higher NA values the trapping depth is reduced due to spherical aberrations. While it is possible to increase the trapping depth [4] by adjusting the objective's tube length this approach is incompatible with our trapping arrangement. A 0.25 NA condenser objective refocuses the scattered laser light and also provide an aperture for an imaging LED to illuminate the focal plane. Samples are loaded onto a piezo driven table to that is inserted between the trapping and condensing objectives; the piezo drivers allow for sub-micron control of the sample position to a degree as small as a 10 nm. To detect and monitor the position of a trapped particle a quadrant photo diode (QPD) was utilised.

### 3.1.1 Position detection methods

In order to accurately capture the dynamics of a trapped particle, a position detection system is utilised. There are 3 possible methods of position detection: video-analysis, lateral-effect position sensing, and photodiodes. The former being ideally suited for multiple traps or situations where precision is not the top priority. In order to match the force measurements of back-focal plane interferometry requires the camera's frame rate to exceed 1 *k*Hz which can be difficult to achieve while maintaining a decent res-

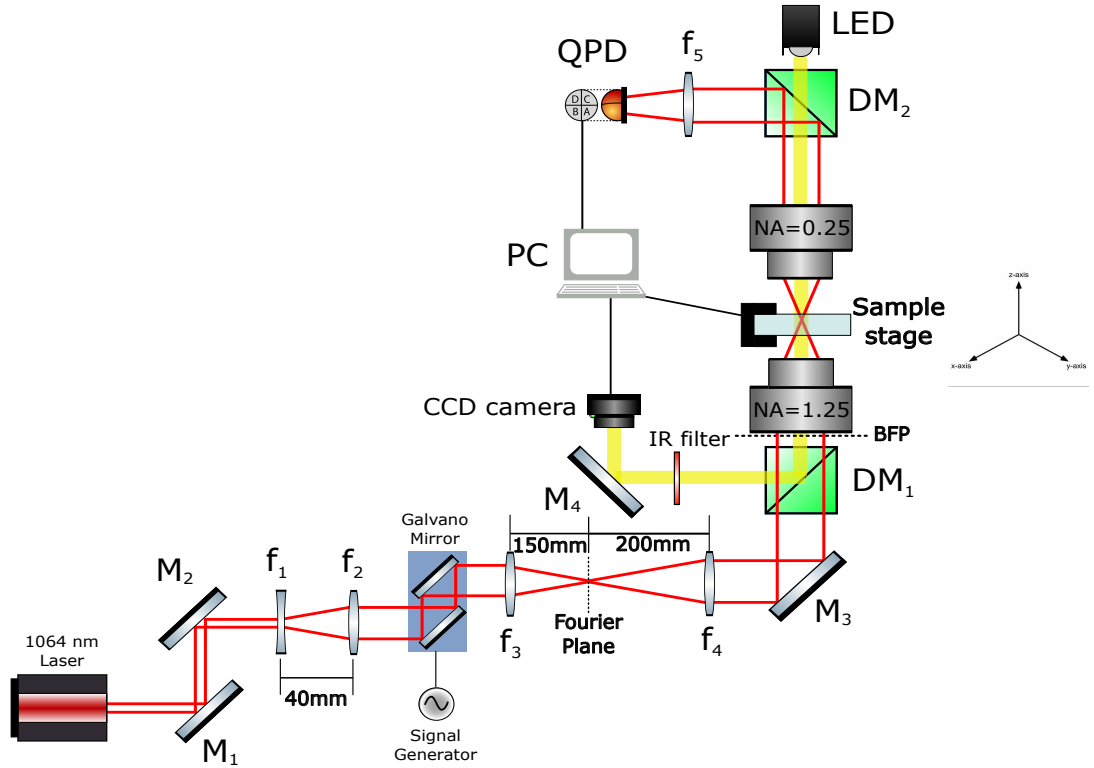


Figure 3.1: Optical tweezer set up used for the majority of the PhD. The focal lengths of  $f_1$ ,  $f_2$ ,  $f_3$ , &  $f_4$  are  $-20\text{ mm}$ ,  $60\text{ mm}$ ,  $150\text{ mm}$ , &  $200\text{ mm}$  respectively. Diagram not drawn to scale.

olution [5]. In comparison off the shelf back-focal plane detectors can achieve temporal resolutions anywhere from  $10 - 100 \text{ kHz}$  [6].

A QPD is frequently used position detection system for optical tweezers due to their high sampling rate, high degree of precision, and ease of set up. The QPD is constructed of four photo diodes assembled in a quadrant formation, when a particle is trapped the interference pattern produced is focused onto the QPD, with the maximum intensity mapping to the particle's centre of mass. By summing the voltages of the horizontal and vertical quadrants together the particle's centre of mass is tracked in the x-y plane. Axial displacement can be estimated by observing the change in the total voltage of the

QPD. The outputted signal gives an indication of the particle's relative displacement from the beam focus, but in order to convert the signal to distance units the trap needs to be calibrated (assuming a linear response curve).

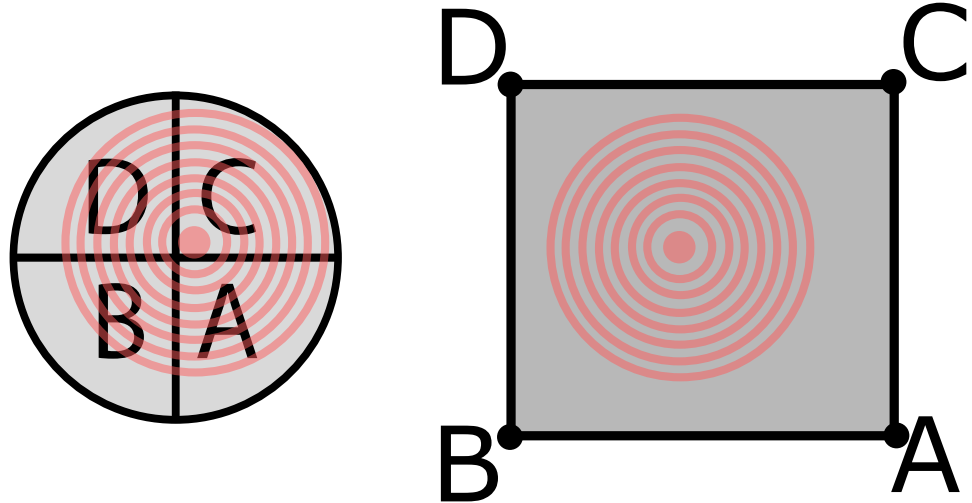


Figure 3.2: Comparison between QPD and Lateral effect photodiodes. The four quadrants of a QPD (left) experience different photocurrents based on the total intensity of light incident on each section (labelled A, B, C, D). Whereas a Lateral effect sensor (right) uses the resistive properties of the photodiode surface to vary the create different photocurrents passing through the anodes A, B, C, and D.

A lateral-effect sensor has a similar output but works using a the entire sensor as a single cell analogous to the focal plane of the trapping beam. The four corners of the sensor act as anodes connected to a base plate cathode, as the beam moves across the surface of the detector each anode will experience a different photocurrent depending on how close the centre of the interference pattern is to each anode. The advantage of

a lateral effect detector is that the linear regime is much larger than a QPD making it much better for monitoring the position of a trapped particle. However, Lateral-effect sensors are often limited in their spacial resolution due to high signal-to-noise ratios, requiring a high intensity of light on the sensor in order to get a clean signal. As a result, most optical trapping experiments are conducted using a QPD as opposed to a lateral-effect sensor, as often the displacement is small enough that the QPD response curve can be considered linear.

### 3.1.2 Fourier Optics and 4f correlators

A 4f correlator is an example of Fourier optics in practice, understanding that a focused lens takes a Fourier transform of the light profile. Consider a laser with a circular Gaussian profile, if you were to place a detector there you would pick up the intensity as a function of its position within the beam. If however you focused the light into a single point (using a +ve focal lens) you are actually seeing a measurement of the phase of your laser with position, in which you would see a diffraction limited spot ( $d = \lambda/2nsin(\theta)$ ), indicating that the laser is collimated. In imaging systems, a series of focal lenses can be used to filter out unwanted scattering from an image (or in an inverse case differentiate between different images), the placement of each lens is shown below.

For our applications a 4f correlator is utilised to ensure that the motion of the galvano-mirrors does not move the focal point of the laser, allowing for a stable trap even while in motion. As shown in Fig. 3.1, after the galvano-mirror we have our two lenses -  $f_3$  and  $f_4$  - the former being installed 150 mm from the second mirror of

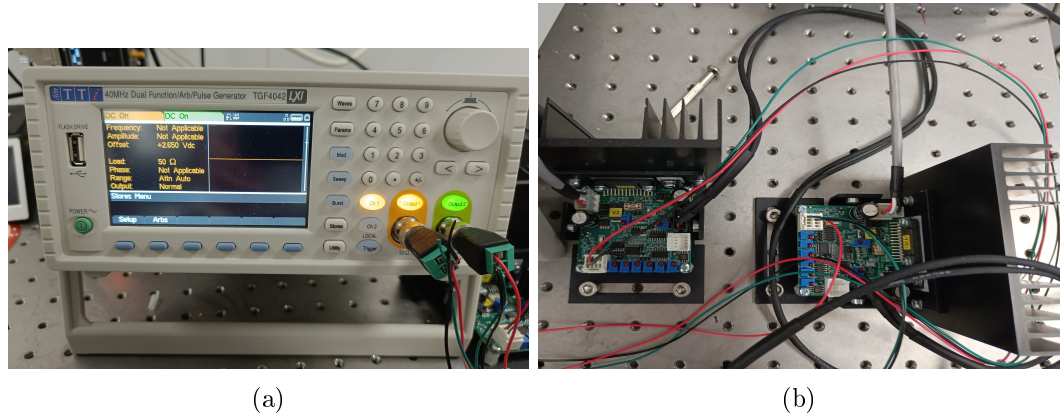


Figure 3.3: Signal generator galvano mirror controller, channel 1 controls the x-axis mirror, while channel 2 controls the y-axis mirror. Both channels can be manipulated independently.

the galvano, and the latter being installed 200 *mm* from the back focal plane of the trapping objective. The signal generator used was supplied by 'MCS Test Equipment Ltd', allowing for dual channel signal control. This allowed us to precisely control the alignment, amplitude, phase, and frequency of both mirrors making alignment much easier. For basic trapping calibration the galvano-mirrors were set to a simple DC output, providing a fixed spot which operates like a typical optical trap.

## 3.2 Synthesis of Birefringent Micro spheres

Generation of fluid shear can be achieved via two avenues: Firstly, by utilising circularly polarised light it is possible to transfer angular momentum from the laser to the trapped entity. Secondly, one can directly move the trap within the imaging plane by steering the beam using either a galvanometric mirror or gimbal mirror. The following chapter outlines the work done with shear generated by circularly polarised light and the challenges of applying this to localising nucleation.

### Chapter 3. Effects of localised shearing on crystal growth and nucleation

There are several options for particles that can be rotated using optical tweezers [7,8].

Over the course of the PhD two different micro spheres where investigated, vaterite and liquid crystal droplets. Both can be readily synthesised in the lab and are will rotate at a variety of sizes. While silver nano particles were considered their high cost and small size meant they were disregarded as an option for optical rotation.

Vaterite is a polymorph of calcium carbonate that is rarely seen in nature due to its low stability. However unlike its other polymorphs of calcite and aragonite, when synthesised vaterite will typically form small spherical particles making them ideal for optical trapping and rotation. Synthesis of vaterite micro spheres requires fine control of the nucleation process in order to maintain polymorphic stability, though for the purposes of optical rotation the exact polymorph is not as important as its morphology as all 3 polymorphs are inherently birefringent.

Vaterite samples where made by the first preparing equal amounts of  $CaCl_2$  and  $Na_2CO_3$  at a concentration of  $0.33M$ , at the same time a vial of  $0.33M\ MgSO_4$  was prepared and set aside for later. First a small vial was filled with  $1.5mL$  of  $CaCl_2$  followed by  $60\mu L$  and  $90\mu L$  of  $MgSO_4$  and  $NaCO_3$  respectively, forming a seed solution. Next, a larger vial was filled with  $5\ mL$ ,  $1.5\ mL$ , and  $1\ mL$  of  $CaCL_2$ ,  $MgSO_4$ , and  $NaCO_3$  respectively followed by the seed solution. After 10 minutes of slow but continuous mixing a few drops of Agepon was added to halt the reaction, the solution was filtered and washed 3 times with distilled water before being suspended in water. When trapped in circularly polarised light, the anisotropic scattering of the sphere results in a periodic signal on the QPD. Therefore, the resulting power spectrum is not a Lorentzian but now also displays peaks that appear at integer multiples of the

particles rotational frequency.

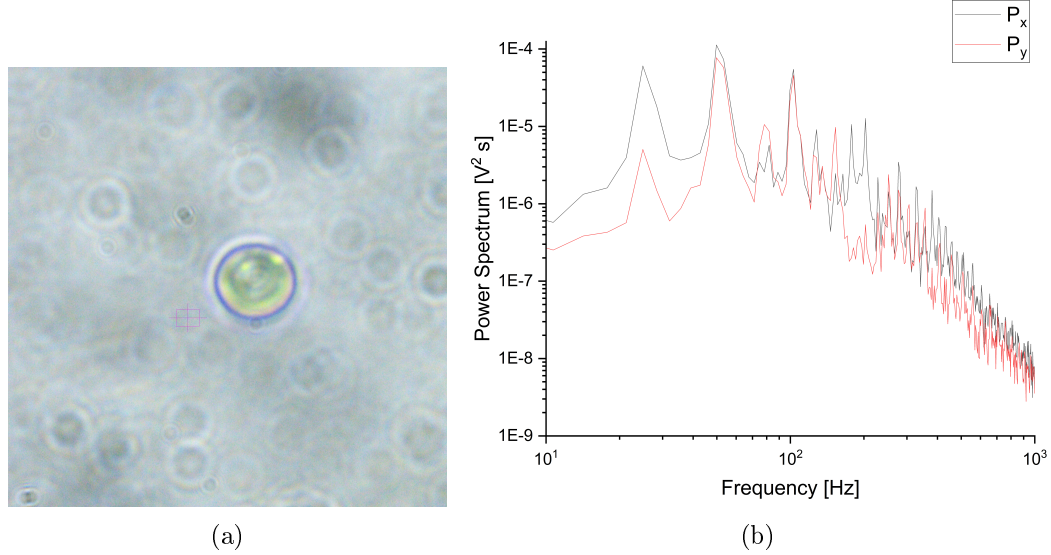


Figure 3.4: (a) Sample vaterite sphere suspended in water and trapped by circular polarised trap. (b) Collected power spectrum from rotating vaterite, peaks in the power spectrum appear at integer multiples of the rotational frequency ( $f_{rot} \approx 49.8$  Hz)

As shown by Fig. 3.4(b) the power spectra produced still demonstrates a Lorentzian curve but modified with these periodic peaks, while the Lorentzian can be loosely fitted to the end tail there exists no current model for describing the power spectra. The closest approximation to this was conducted by [9] where they describe the rotational motion of ellipsoidal polystyrene particles. The critical assumption being that the particle perfectly rotates in the  $x - y$  plane; however it has long been suspected that birefringent microspheres experience random rotations outside of the  $x - y$  plane [10] making it very difficult to characterise the forces on rotating microspheres without a proper understanding of the optical torque being applied to it.

### 3.2.1 Liquid Crystal Rotors

Liquid crystals are an intriguing example of materials with mixed phase properties, unlike typical solutes such as Glycine, a liquid crystal can still maintain some degree of order between its individual molecules while in the liquid state. This is due to the fact that liquid crystals are constructed of long ordered molecules that demonstrate a long range ordering. There are three main types of liquid crystal transition methods: thermotropic crystals will transition to their liquid crystal phase when sufficiently heated; Lyotropic materials can undergo this transition due to changes in temperature and concentration; and lastly Metallotropic materials - which are composed of both organic and inorganic molecules - change phase according to the ratio of organic to inorganic molecules present. Liquid crystal rotors are rather simple in their production, 4-Heptyl-4-biphenylcarbonitrile (7CB) was purchased from Sigma Aldrich and a small amount was added to a vial of distilled water. The solution was then heated in a water bath to 25° in order to transition the solid crystal into its liquid crystal state. The individual droplets are inherently birefringent and rotate in a circularly polarised trap.

The liquid crystal droplets had a much faster rotation rate than comparable vaterite spheres, due to their higher degree of birefringence and the fact that the droplets are far closer to perfect spheres making angular momentum transfer more efficient.

### 3.2.2 Rotation of birefringent micro spheres

Optical tweezing has often been used for micro-rheology, by computing the exact forces being exerted on the trapped sphere, one can determine the local temperature/viscosity

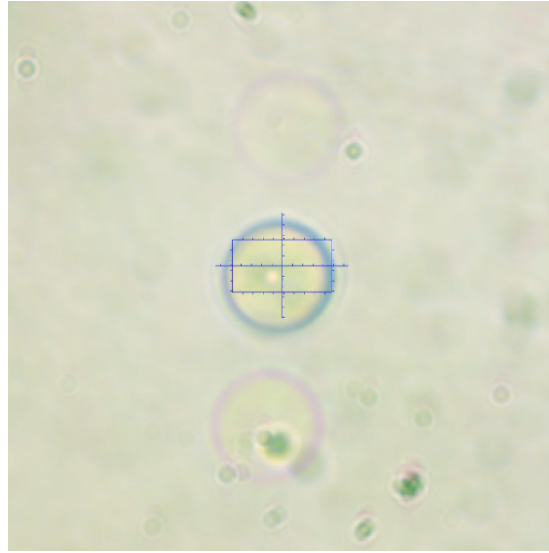


Figure 3.5: Liquid crystal undergoing rotation due to the circularly polarised trap.

of the medium [11, 12]. Using a birefringent particle and rotating it within the fluid, the maximum rotation rate is due to the fluid drag resisting the torque of the trapping beam [12]. If you want to measure fluid flow you can instead use a micro-rotor to see how fluid flow propagates in the medium [13]. Likewise, one can use a galvanometric mirror to probe the drag force of the fluid, by understanding the trap strength (calibrating using a low frequency signal) one can measure the drag force experienced by the local fluid [14]. I

Understanding the fluid velocity around our trapped object is determined mostly by the Reynold's number of our system, for a sphere submersed in a moving fluid of velocity  $U$  this is given by:

$$Re = \frac{\rho U D}{\mu} \quad (3.2)$$

Where  $D$  is the sphere's diameter, and  $\rho$  and  $\mu$  are the fluid's density and viscosity

respectively. In our case we do not have a fluid moving around a sphere but a sphere moving through the fluid at some velocity  $U$ , assuming a no-slip boundary condition we can model the fluid velocity profile based on the velocity of the particle. There are two possible avenues for generating shear flow with a trapped particle; rotation of birefringent particles, and fluid flow induced by particle motion.

Rotating birefringent particles are by far the most common method for generating and measuring fluid flow in a solution. To see if we can even achieve the theoretical maximum shear rate, vaterite spheres were synthesised (see Sec.3.2) submerged in water and trapped with the 1064 nm laser at set to 450 mW. The rotation frequency was determined using the QPD, and the particle sizes were computed by image analysis. With the particle size and rotation frequency, the tangential rotation speed is calculated via:

$$u(r) = \frac{\pi}{4} \frac{d^3}{r^2} \omega \quad (3.3)$$

Where  $d$  is the particle diameter,  $\omega$  is the rotation frequency reported by the QPD, and  $r$  is the distance from the particle's centre. Using Eq.3.3 we computed the fluid flow radiating outward from the centre of the sphere. The shear rate can then be computed as the partial derivative fluid flow (assuming shearing is generated purely by the flow field):

$$\dot{\gamma}(r) = \left| \frac{\delta u(r)}{\delta r} \right| = \frac{\pi}{2} \frac{d^3}{r^3} \omega \quad (3.4)$$

First we tested the rotational behaviour of vaterite in distilled water, samples of vaterite where diluted down and  $200\mu L$  was pipetted onto the sample stage. Due to Van der Waal's forces some of the microspheres were stuck together, fortunately individual sphere's were still present. Over the course of a few weeks multiple sphere's where trapped and their rotation speeds were measured via the QPD.

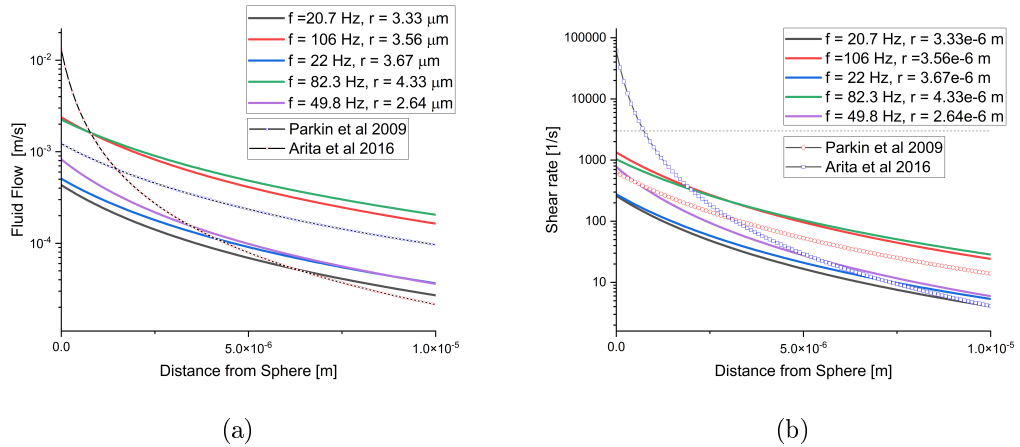


Figure 3.6: (a) Fluid flow radiating out from the surface of a rotating vaterite sphere. (b) Shear rates computed using Eq.3.4, optimal shear rate is of  $3000\text{s}^{-1}$  is indicated by the dotted line. Vaterite radii and rotation frequencies are shown, the laser power was kept constant at 450 mW. Reported rotation rates, and their corresponding fluid flow and shear rates, for vaterite are also plotted alongside lab results.

From Fig.3.6 there is not a strong relationship between particle size and rotation rate, this is contrary to much of the theoretical predictions that predict an exponential decay with particle size. This can be in part due to the fact that synthesising perfectly spherical spheres that have uniform birefringence is difficult over multiple experiments and tests. Despite our best efforts at controlling the growth rate the vaterite spheres would often combine together while suspended in water after a short period of time. The fastest reported rotation rate found during this PhD was by [15] that achieved a rotation rate of  $5 \text{ kHz}$ , this is plotted on Fig 3.6 as the dotted line. Even at that

extreme a rotation rate the region in which nucleation is at its optimal likelihood is only 20 nm wide meaning that localising nucleation around a rotating sphere is vanishingly small.

### 3.3 Rotation of micro-rotors in supersaturated solutions

Vaterite samples were synthesised according to [7,16] (see sec. 3.2), and then suspended in distilled water, at the same time a supersaturated solution of Glycine and water was prepared and 50  $\mu L$  was pipetted onto a glass cover slip. A single microsphere the vaterite was trapped in a circularly polarised light and brought close to the droplet edge.

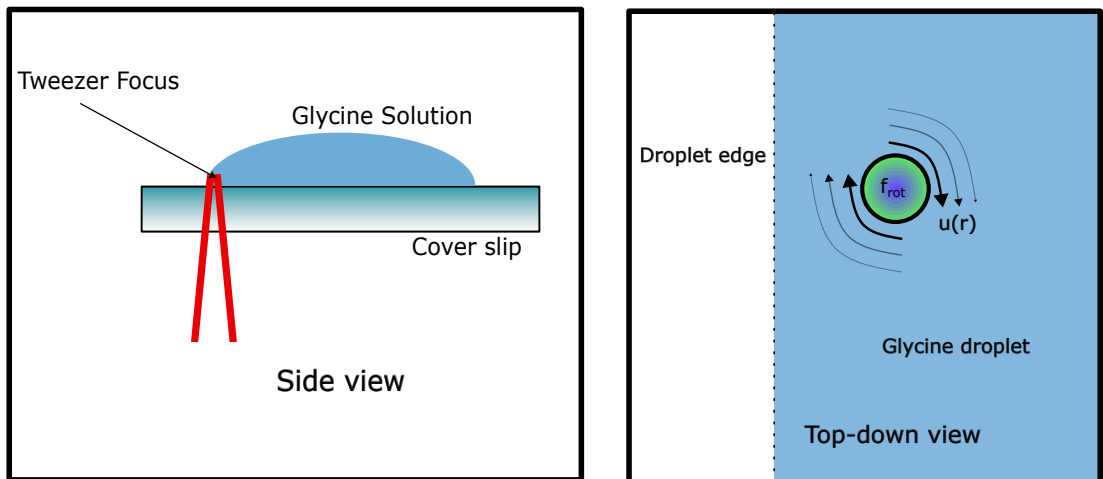


Figure 3.7: Diagram of optical trapping set up for rotating birefringent particles in a supersaturated solution. Left: side view of the trapping set up showing the location of the trap focus at the edge of the droplet of a supersaturated solution. Right: top down view of the glycine droplet with a trapped birefringent particle shown close to edge of the trap. As the particle rotates the drag force from the surrounding fluid generates a flow field around itself (see Eq. 3.3).

After a period of ten minutes if no nucleation event was observed the particle was released and another particle was trapped. Due to the increased viscosity of the super-

### Chapter 3. Effects of localised shearing on crystal growth and nucleation

saturated solution and the proximity to the droplet edge, as previous works have only seen nucleation near the solution-air interface [17–19], the observed rotation rate was rather low or non-existent, the results are tabulated below:

Table 3.1: Results from rotating vaterite within supersaturated solution of  $H_2O$  and Glycine. Solubility concentration for Glycine at  $16^\circ$  was  $C^* = 0.2016g/g$

Super Saturation	Particle radius [ $\mu$ ]	$\omega$ [Hz]	Nucleation [✓/✗]
1.01	2.34	20.7	✗
	5.67	23.3	✗
	3.26	15.4	✗
1.14	1.89	1.23	✗
	3.75	3.54	✗
	4.35	4.86	✗
1.4	3.47	0.00	✗
	1.59	0.00	✗
	6.24	0.00	✗
1.45	6.32	0.00	✗
	3.68	0.00	✗
	5.43	0.00	✗
1.49	4.76	0.00	✗
	7.27	0.00	✗
	1.52	0.00	✗

The calculations from fig.3.6 indicate that even in pure water the rotational speed achieved by a microsphere is insufficient to achieve a significant shear rate more than a few tenths of a microns from its surface. The closest we could trap a microsphere to the droplet edge was in the range of  $5\text{--}10\mu m$ , at that distance the fluid flow would be so low that not even using a liquid droplet rotor would achieve the rotational speeds necessary to localise nucleation. While in theory a sufficiently focused laser could rotate any microsphere to a fast enough to match the speeds expected by [1] the localised intensity would be so large that even using  $D_2O$  would see a significant increase in temperature.

It is not impossible that fluid shearing could be used in the future to localise nu-

cleation; but from these results, using individual micro-rotors do not seem like an appropriate method. If multiple micro-rotors could be trapped in close proximity to one another they could create a large region of fluid where nucleation is more likely than the bulk fluid. Micro-rotors have been created that allow for precise control of suspended micro-particles [20] and could potentially be used to generate sufficient shearing, however these could not be used in this PhD as we lacked the necessary hardware to form multiple gradient traps.

### 3.4 Shearing via a Galvano-mirror

Rather than utilising birefringence rotation, which is subject to issues during synthesis and achieving an ideal particle size, a galvano-mirror was installed to induce controlled particle motion. While typically galvano and gimble mirrors are used to trap multiple particles in a regular pattern, in a sufficiently dilute solution a single silica micro sphere can be moved quickly through a fluid along a preset path. Calculating the shear rate around an individual particle is difficult to do precisely but for low Reynolds numbers we can get an adequate approximation.

For a simple circular path one can estimate the sphere's speed by the radius of its path and the frequency of its orbit  $U = R\omega$ ; however for a more complex path, such as an elliptical orbit the curve needs to be parametrised. One can describe the position parameter of a circular path as such:

$$r(u) = [r\cos(2\pi u), r\sin(2\pi u), 0] \quad (3.5)$$

If we say that  $u$  describes time from some initial point we can say  $u = t\omega$  where  $\omega$  is the frequency of orbit. Substituting this in and then taking the partial derivative of position gives:

$$v(t) = \frac{dr(t)}{dt} = [-2\pi r\omega \sin(2\pi t\omega), 2\pi r\omega \cos(2\pi t\omega), 0] \quad (3.6)$$

In order to compute  $U$  we simply take the magnitude of our velocity. For low velocities the fluid flow at the sphere's surface can be computed based on its velocity.

$$u_r(r) = -|v(t)|^2 \cos(\theta) \left( 1 - \frac{3R}{2r} + \frac{R^3}{2r^3} \right) \quad (3.7)$$

Where  $\theta$  is the angle from the direction of movement to the point you wish to measure, and  $r$  is the radial distance to that point. Again taking the partial derivative we can get the shear rate for a particle moving through the fluid:

$$\dot{\gamma}(r) = \left| \frac{\delta u_r(r)}{\delta r} \right| = |v(t)|^2 \cos(\theta) \left( \frac{3R}{r^2} - \frac{2R^3}{r^4} \right) \quad (3.8)$$

Moving a silica bead along a circular path can generate significant fluid flow around a larger volume compared to comparable microspheres.

### 3.5 Nucleation using a moving beam

As mentioned previously, shearing via optical rotation and particle displacement did not result in any localised nucleation events even while in the proximity of the droplet edge.

During the experiments with the galvano-mirror, it was found that when no particle was present in the optical trap nucleation events would occur while the beam was close to the edge of the droplet, even though the solution was undersaturated. This has been reported prior [18, 21], but was more interesting is how the beam's motion influenced the growth of the nucleus.

Consider below in Fig. 3.8 the frames taken from a nucleation event in supersaturated glycine solution ( $S = 1.03$ ), the beam is a stationary being  $\approx 3.5\mu m$  from the droplet edge. After a period of roughly 5 minutes a nucleus forms at the trap focus, growing quickly (growth rate was approximated using imageJ to be on the order of  $700 \mu m^2/min$ ) from the focal point of the trap until after roughly 6 seconds the crystal escapes. Comparing to previous literature using optical tweezers shows that the growth rate is only loosely connected to the solutions supersaturation, local conditions play a much larger role in the growth rate than just the concentration [22]. A likely reason that the trap is escaped is due to the fact that crystal is far too large to be held in place and is in fact still growing as the solution is supersaturated. The key take away to remember is that the beam has no real influence over the crystal shape, instead it

grows outward from the trap focus.

Now while trying to induce fluid flow by optically trapping a silica particle and using a galvano-mirror to move the particle through the solution, nucleation events were observed in which crystal growth follows the laser focus. Shown below in Fig. 3.9 where we have the laser focus moving in a small elliptical pattern; interestingly, due to the addition of the silica suspension we see the presence of small spheres, these appear too small to be silica beads which have a uniform radius of  $1.57 \mu m$ , we surmise these could be small clusters of Glycine that had previously been shown to form when the aqueous solutions where irradiated with a focused laser [17,23]. While no droplets are seen directly entering the focus a nucleus forms close to the droplet edge, unlike in Fig. 3.8 the crystal does not grow out from the focal point evenly; due to the galvano mirror, the crystal is simultaneously being moved by and growing around the focal point of the trap. Because of this the crystal nucleus lacks a clear morphology at first, until roughly  $20 s$  the crystal reaches a almost prismatic structure, with further irradiation increasing the size. Interestingly the galvano-mirror allows the trap to impart a slight torque on the crystal, as shown in fig. 3.9(c) and (d), where even though the crystal is not directly in the trap focus it rotates in the  $x - y$  plane and gets trapped again at a corner. The rotation could not be due to fluid flow close to the surface of the crystal as trap should have no influence on fluid molecules smaller than a few hundred nano-meters. In figs.3.9(e) and (f), the crystal growth is localised to the corner, even though previously the crystal growth was roughly uniform (compare figs. 3.9(b) and (c)). The area growth rate between figures 3.9(a) and (d) was approximated using imageJ at  $45.03 \mu m^2/min$ , where as between figures 3.9(e) and (f) the growth rate at

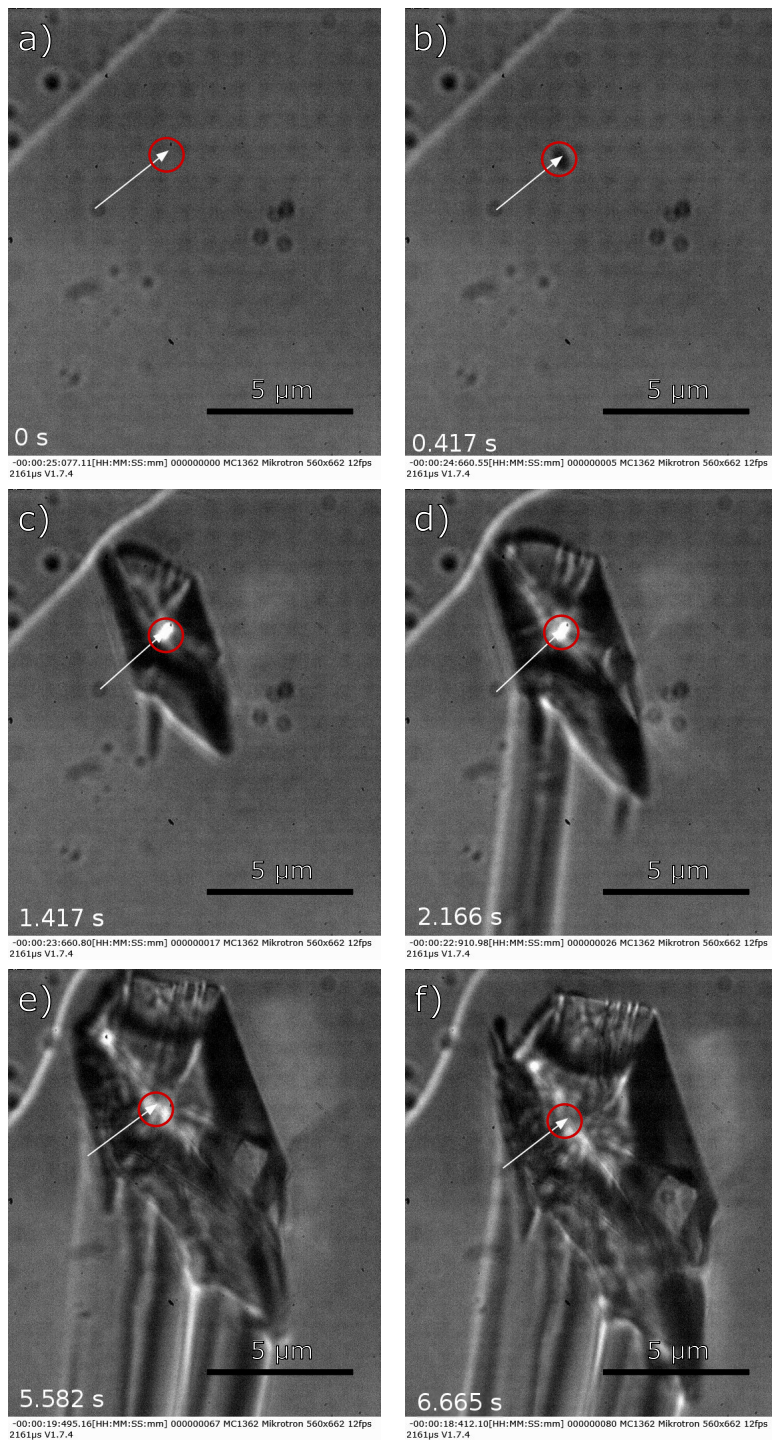


Figure 3.8: Laser induced nucleation at the edge of a droplet of supersaturated glycine solution. (b) shows the first instance of a crystal nucleus, growing quickly through (c)-(e) until after 6.665 s the crystal begins to escape the trap.

Chapter 3. Effects of localised shearing on crystal growth and nucleation

that particular edge was estimated at  $42.10 \mu\text{m}^2/\text{min}$ .

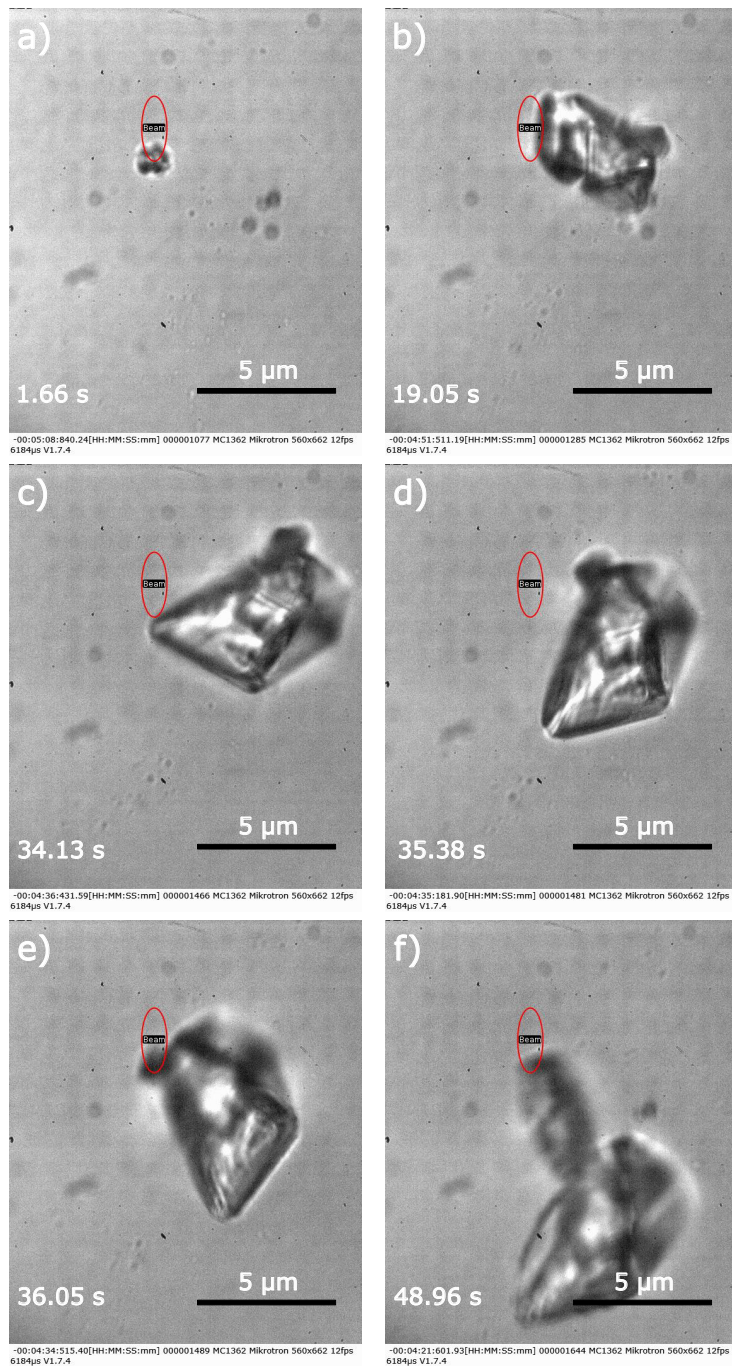


Figure 3.9: Laser induced nucleation at the edge of a droplet of supersaturated glycine solution. (b) shows the first instance of a crystal nucleus, growing quickly through (c)-(e) until after 6.665 s the crystal begins to escape the trap.

In this instance  $20 \mu L$  of glycine and water ( $S = 1.03$ ) was added to  $10 \mu L$  of a dilute water-silica mixture making the solution undersaturated ( $S \approx 0.7$ ). Nucleation in undersaturated conditions has been reported previously in  $D_2O$  [21] and  $H_2O$  [22]. Though notably in both cases the crystal morphology is not influenced by the location of the laser focus, it has been shown that polarisation can influence the polymorphic control for simple salts [24, 25] but no research has been done into the influence of a moving beam front on the growth of a newly formed nucleus.

### 3.6 Influence of a moving beam front on seed crystals

To see if the above phenomena had any direct influence on a

# Bibliography

- [1] R. Debuyschère, B. Rimez, A. Zacccone, and B. Scheid, “Experimental and theoretical investigation of nonclassical shear-induced nucleation mechanism for small molecule,” *Crystal Growth & Design*, vol. 23, no. 7, pp. 4979–4989, Jun. 2023.
- [2] F. Mura and A. Zacccone, “Effects of shear flow on phase nucleation and crystallization,” *Physical Review E*, vol. 93, no. 4, p. 042803, Apr. 2016.
- [3] H.-I. Kim, I.-J. Joo, S.-H. Song, P.-S. Kim, K.-B. Im, and C.-H. Oh, “Dependence of the optical trapping efficiency on the ratio of the beam radius-to-the aperture radius,” *Journal of the Korean Physical Society*, vol. 43, no. 3, p. 348, 2003.
- [4] S. N. S. Reihani, M. A. Charsooghi, H. R. Khalesifard, and R. Golestanian, “Efficient in-depth trapping with an oil-immersion objective lens,” vol. 31, p. 766, 2006.
- [5] G. M. Gibson, J. Leach, S. Keen, A. J. Wright, and M. J. Padgett, “Measuring the accuracy of particle position and force in optical tweezers using high-speed video microscopy,” *Optics Express*, vol. 16, no. 19, p. 14561, Sep. 2008.

## Bibliography

- [6] K. Berg-Sørensen and H. Flyvbjerg, “Power spectrum analysis for optical tweezers,” vol. 75, pp. 594–612, 2004.
- [7] S. J. Parkin, R. Vogel, M. Persson, M. Funk, V. L. Loke, T. A. Nieminen, N. R. Heckenberg, and H. Rubinsztein-Dunlop, “Highly birefringent vaterite microspheres: production, characterization and applications for optical micromanipulation,” *Optics Express*, vol. 17, no. 24, p. 21944, Nov. 2009.
- [8] K. Saito and Y. Kimura, “Optically driven liquid crystal droplet rotator,” *Scientific Reports*, vol. 12, no. 1, Oct. 2022.
- [9] Yugesha, S. Bhattacharya, and S. Ananthamurthy, “Characterizing the rotation of non symmetric objects in an optical tweezer,” *Optics Communications*, vol. 285, no. 10–11, pp. 2530–2535, May 2012.
- [10] J. Bang, T. Seberson, P. Ju, J. Ahn, Z. Xu, X. Gao, F. Robicheaux, and T. Li, “Five-dimensional cooling and nonlinear dynamics of an optically levitated nanodumbbell,” *Physical Review Research*, vol. 2, no. 4, p. 043054, Oct. 2020.
- [11] J. Millen, T. Deesuwan, P. Barker, and J. Anders, “Nanoscale temperature measurements using non-equilibrium brownian dynamics of a levitated nanosphere,” *Nature Nanotechnology*, vol. 9, no. 6, pp. 425–429, May 2014.
- [12] P. Rodríguez-Sevilla, Y. Arita, X. Liu, D. Jaque, and K. Dholakia, “The temperature of an optically trapped, rotating microparticle,” *ACS Photonics*, vol. 5, no. 9, pp. 3772–3778, Aug. 2018.

## Bibliography

- [13] G. Knöner, S. Parkin, N. R. Heckenberg, and H. Rubinsztein-Dunlop, “Characterization of optically driven fluid stress fields with optical tweezers,” *Physical Review E*, vol. 72, no. 3, p. 031507, Sep. 2005.
- [14] R. M. Robertson-Anderson, “Optical tweezers microrheology: From the basics to advanced techniques and applications,” *ACS Macro Letters*, vol. 7, no. 8, pp. 968–975, Aug. 2018.
- [15] Y. Arita, J. M. Richards, M. Mazilu, G. C. Spalding, S. E. Skelton Spesvvtseva, D. Craig, and K. Dholakia, “Rotational dynamics and heating of trapped nanovaterite particles,” *ACS Nano*, vol. 10, no. 12, pp. 11 505–11 510, Dec. 2016.
- [16] A. I. Bishop, T. A. Nieminen, N. R. Heckenberg, and H. Rubinsztein-Dunlop, “Optical microrheology using rotating laser-trapped particles,” *Physical Review Letters*, vol. 92, no. 19, p. 198104, May 2004.
- [17] O. Y. Gowayed, T. Moosa, A. M. Moratos, T. Hua, S. Arnold, and B. A. Garetz, “Dynamic light scattering study of a laser-induced phase-separated droplet of aqueous glycine,” vol. 125, pp. 7828–7839, 2021.
- [18] Z. Liao and K. Wynne, “A metastable amorphous intermediate is responsible for laser-induced nucleation of glycine,” vol. 144, pp. 6727–6733, 2022.
- [19] F. Walton and K. Wynne, “Control over phase separation and nucleation using a laser-tweezing potential,” vol. 10, pp. 506–510, 2018.

## Bibliography

- [20] U. G. Būtaitė, G. M. Gibson, Y.-L. D. Ho, M. Taverne, J. M. Taylor, and D. B. Phillips, “Indirect optical trapping using light driven micro-rotors for reconfigurable hydrodynamic manipulation,” *Nature Communications*, vol. 10, no. 1, Mar. 2019.
- [21] T. Rungsimanon, K. ichi Yuyama, T. Sugiyama, and H. Masuhara, “Crystallization in unsaturated glycine/d<sub>2</sub>o solution achieved by irradiating a focused continuous wave near infrared laser,” vol. 10, pp. 4686–4688, 2010.
- [22] J. Flannigan, “Optical tweezer and particle control of nucleation and growth at the microscale,” Ph.D. dissertation, University of Strathclyde, 2023. [Online]. Available: <https://pureportal.strath.ac.uk/en/studentTheses/optical-tweezer-and-particle-control-of-nucleation-and-growth-at->
- [23] Y. Tsuboi, T. Shoji, and N. Kitamura, “Optical trapping of amino acids in aqueous solutions,” *The Journal of Physical Chemistry C*, vol. 114, no. 12, pp. 5589–5593, Dec. 2009.
- [24] B. A. Garetz, J. E. Aber, N. L. Goddard, R. G. Young, and A. S. Myerson, “Non-photochemical, polarization-dependent, laser-induced nucleation in supersaturated aqueous urea solutions,” *Physical Review Letters*, vol. 77, no. 16, pp. 3475–3476, Oct. 1996.
- [25] B. A. Garetz, J. Matic, and A. S. Myerson, “Polarization switching of crystal structure in the nonphotochemical light-induced nucleation of supersaturated aqueous glycine solutions,” *Physical Review Letters*, vol. 89, no. 17, p. 175501, Oct. 2002.